Applied Catalysis B: Environmental 274 (2020) 118963

Contents lists available at ScienceDirect

Applied Catalysis B: Environmental

journal homepage: www.elsevier.com/locate/apcatb

Size effect, mutual inhibition and oxidation mechanism of the catalytic removal of a toluene and acetone mixture over TiO_2 nanosheet-supported Pt nanocatalysts

Zhiwei Wang[a], Peijie Ma[b], Kun Zheng[b], Can Wang[c], Yuxi Liu[a], Hongxing Dai[a], Chongchen Wang[d], Hsing-Cheng Hsi[e], Jiguang Deng[a,*]

[a] Key Laboratory of Beijing on Regional Air Pollution Control, Beijing Key Laboratory for Green Catalysis and Separation, College of Environmental and Energy Engineering, Beijing University of Technology, Beijing, 100124, China
[b] Beijing Key Lab. of Microstructure and Properties of Advanced Materials, Institute of Microstructure and Properties of Advanced Materials, Beijing University of Technology, Beijing, 100124, China
[c] Tianjin Key Lab of Indoor Air Environmental Quality Control, School of Environmental Science and Engineering, Tianjin University, Tianjin, 300072, China
[d] Beijing Key Laboratory of Functional Materials for Building Structure and Environment Remediation, Beijing University of Civil Engineering and Architecture, Beijing, 100044, China
[e] Graduate Institute of Environmental Engineering, National Taiwan University, Taipei, Taiwan

ARTICLE INFO

Keywords:
Supported Pt nanocatalyst
Toluene and acetone mixture
Size effect
Mutual inhibition
Catalytic oxidation mechanism

ABSTRACT

We prepare TiO_2 nanosheet-supported Pt nanocatalysts with an average size of 1.3, 1.9, and 3.0 nm. Due to the great decrease in the adsorption ability for toluene and acetone, mutual inhibition is first observed over $Pt_{1.9\,nm}/TiO_2$ for the catalytic removal of a toluene and acetone mixture. At 140 °C, the toluene and acetone reaction rate is 0.033 and 0.045 μmol/(g_{cat} s), respectively, for the oxidation of 500 ppm toluene or acetone, which is much higher than the corresponding reaction rate (0.020 and 0.007 μmol/(g_{cat} s)) for the oxidation of the mixture. $Pt_{1.9\ nm}/TiO_2$ exhibits a good catalytic stability and H_2O and CO_2 tolerance. With strong evidence, we find that the co-presence of toluene and acetone does not change the catalytic mechanism, and the reaction pathway for the oxidative removal of toluene and acetone in the mixture may follow the pathway for the oxidation of single toluene or acetone.

1. Introduction

Volatile organic compounds (VOCs) emitted from industrial sources could cause serious environmental problems, such as photochemical smog, an ozone hole, and smog [1,2]. Moreover, most VOCs are harmful to human health [3,4] (damage the respiratory system and central nervous system and are carcinogenic, teratogenic and mutagenic). Hence, it is urgent to control the emission of VOCs. The traditional methods used for the abatement of VOCs include physical [5–7] (e.g., absorption, adsorption, and membrane separation) and chemical [8–18] (e.g., photocatalysis, photothermal synergy, and catalytic oxidation) methods. Because of its high removal rate, low energy consumption, and no secondary pollution, catalytic oxidation is considered one of the most efficient techniques for the degradation of low concentration VOCs. Recently, many reviews on the catalytic oxidation of VOCs could be found in the literature [19,20], and we find that it is highly necessary to develop a catalyst with a high efficiency, high quality and low price. Up to now, supported noble metal (especially Pt) [21–24] catalysts are widely used for the catalytic degradation of VOCs due to their good catalytic performance at low temperatures. However, there are many factors (e.g., the particle size of Pt) affecting the catalytic activity of Pt catalysts. In recent years, many researchers have performed many studies to investigate the size effect of Pt in the field of electrocatalysis [25–30], photocatalysis [31,32], and dehydrogenation/hydrogenation [33–35]. However, studies about the effect of the Pt size on the abatement of VOCs are scarce.

As we know, real industrial emissions usually contain various kinds of VOCs. For example, 32 kinds of volatile organic compounds (VOCs) are detected in the concentrated areas of pharmaceutical companies in Shijiazhuang City, Hebei Province, China [36]. Furthermore, ketones and aromatic hydrocarbons account for the highest proportion due to the extensive use of organic solvents such as toluene and acetone in the pharmaceutical process. Although catalytic oxidation is widely investigated for the abatement of single VOCs, such as toluene, o-xylene,

* Corresponding author.
E-mail address: jgdeng@bjut.edu.cn (J. Deng).

https://doi.org/10.1016/j.apcatb.2020.118963
Received 30 January 2020; Received in revised form 28 March 2020; Accepted 1 April 2020
Available online 20 April 2020
0926-3373/

benzene, acetone and formaldehyde [37–40], few studies on the catalytic oxidation of VOC mixtures could be found [41–45]. Actually, both inhibiting and promoting effects are observed for the catalytic oxidation of VOC mixtures. For example, Beauchet et al. [41] observed that o-xylene strongly inhibits isopropanol oxidation performed over basic NaX zeolites due to the adsorption of o-xylene around the pore of zeolite, which limits isopropanol from accessing the active sites. Moreover, the by-products of isopropanol oxidation were influenced by the concentration of o-xylene. He et al. [45] observed a promoting effect, in which the introduction of ethyl acetate accelerated the oxidation of toluene due to the exothermic character of the complete oxidation reaction, leading to the rise in the surface temperature of the catalysts.

In recent years, it is highly desired to remove VOCs due to the strictness of industrial emissions in China. As abovementioned, few studies on the catalytic oxidation of VOC mixtures could be found in the literature, while real industrial emissions usually contain various kinds of VOCs. Therefore, it is highly necessary to explore the catalytic oxidation of VOC mixtures. In the present study, we first prepare a series of Pt/TiO_2 catalysts with different particle sizes via the chemical reduction strategy and investigate the size effect on the catalytic activity for toluene oxidation. Subsequently, we investigate the catalytic performance of the Pt/TiO_2 (the average Pt particle size = 1.9 nm) catalyst, including the activity, thermal stability, and the effect of H_2O and CO_2, for the oxidation of toluene and acetone mixtures, a typical emission from the pharmaceutical industry. The significant contributions of this manuscript include the following: (1) we first report the mutual inhibition of the catalytic removal of a toluene and acetone mixture and clarify the reason that the co-presence of toluene and acetone weakens the adsorption ability of the Pt/TiO_2 nanocatalyst; and (2) we propose the catalytic mechanism of the oxidative removal of the toluene and acetone mixture over the Pt/TiO_2 nanocatalyst in detail and present strong support via various online characterization studies.

2. Experiment

2.1. Catalyst preparation

Tetrabutyl titanate (98 %), $H_2PtCl_6.6H_2O$ (Pt ≥ 35 %), HF (40 %), ethylene glycol (99.0 %), NaOH (96.0 %), methanol (99.5 %), and polyvinyl pyrrolidone (PVP, K30) are purchased from Sinopharm Chemical Reagent Co., Ltd. and used as received without further purification.

The TiO_2 nanosheet is prepared according to a modified hydrothermal method [46]. First, 5 mL HF and 25 mL $Ti(OC_4H_9)_4$ are mixed in a Teflon autoclave (100 mL) under vigorous magnetic stirring for 10 min, and then, the autoclave is heated in an oven at 190 °C for 24 h. The white precipitate is washed ten times by distilled water and ethanol to remove the residual HF and then dried at 80 °C for 12 h. The TiO_2 nanosheet is obtained after calcination at 550 °C for 2 h. The Pt nanoparticles (NPs) with different sizes are prepared by a chemical reduction method [47,48]. A detailed preparation process is described in the Supporting Information (SI). The average particle size of the Pt NPs in the solution is 1.2, 1.7, and 2.9 nm (Fig. S1). A certain amount of the Pt solution (theoretical loading = 0.15 wt%) and 2 g TiO_2 nanosheets are dispersed in 150 mL water under vigorous stirring for 12 h, and then, the slurry is washed several times with hot deionized water and ethanol. The Pt/TiO_2 catalysts are obtained after calcination at 350 °C for 3 h. It should be noted that possibly due to the thermal treatment performed in the muffle furnace, the average particle size of the Pt NPs slightly increases to 1.3, 1.9, and 3.0 nm after the particles are loaded on the TiO_2 nanosheet support. Accordingly, the obtained catalysts are defined as $Pt_{1.3\,nm}/TiO_2$, $Pt_{1.9\,nm}/TiO_2$, and $Pt_{3.0\,nm}/TiO_2$. The real loading of Pt in the $Pt_{1.3\,nm}/TiO_2$, $Pt_{1.9\,nm}/TiO_2$, and $Pt_{3.0\,nm}/TiO_2$ catalysts is 0.12, 0.12, and 0.13 wt% (Table S1), respectively.

2.2. Catalyst characterization

The physicochemical properties of the catalysts are investigated by using X-ray diffraction (XRD), transmission electron microscopy (TEM), aberration-corrected high-angle annular darkfield scanning transmission electron microscopy (A C-H AADF-STEM), inductively coupled plasma atomic emission spectroscopy (ICP-AES), X-ray photoelectron spectroscopy (XPS), the Brunauer-Emmett-Teller (BET) technique, VOC-temperature programmed desorption (VOC-TPD), VOC-temperature programmed oxidation (VOC-TPO), thermal desorption analysis (TD)-online GC/MS, and *in situ* diffuse reflectance infrared Fourier transform spectroscopy (*in situ* DRIFTS). The detailed characterization procedures are described in the SI.

2.3. Catalytic performance evaluation

The catalytic activity of the catalyst for VOC (toluene or/and acetone) oxidation is evaluated in a micro-fixed bed reactor (inner diameter = 6 mm). To avoid the hot runaway phenomenon, 50 mg catalyst (40–60 mesh) and 250 mg silicon (40–60 mesh) are fixed in the reactor. The typical reaction conditions are x ppm toluene + y ppm acetone ($x + y = 1000$; $x = 0$, 200, 500, 800, and 1000) + 20 % O_2 + N_2 (balance gas), in which the weight hourly space velocity (WHSV) = 40,000 mL/(g h). Furthermore, the thermal stability and effect of H_2O and CO_2 on the catalytic oxidation of the toluene and acetone mixture are also investigated. The detailed evaluation procedures are described in the SI.

3. Results and discussion

3.1. Size effect on the catalytic activity of Pt/TiO_2 for toluene oxidation

As mentioned in the introduction, the particle size is an important factor affecting the catalytic activity of the supported Pt catalysts. Herein, the catalytic activities of the $Pt_{1.3\,nm}/TiO_2$, $Pt_{1.9\,nm}/TiO_2$, and $Pt_{3.0\,nm}/TiO_2$ catalysts for complete toluene oxidation are evaluated under the typical reaction condition (Fig. S2A). Generally, toluene conversion increases with a rise in the reaction temperature, and $Pt_{1.9\,nm}/TiO_2$ performs better than $Pt_{1.3\,nm}/TiO_2$ and $Pt_{3.0\,nm}/TiO_2$. To better compare the catalytic activity, $T10$ %, $T50$ %, and $T90$ % (the temperature required for 10 %, 50 %, and 90 % conversion) are listed in Table S2. $T90$ % over $Pt_{1.3\,nm}/TiO_2$, $Pt_{1.9\,nm}/TiO_2$, and $Pt_{3.0\,nm}/TiO_2$ is 205, 190, and 194 °C, respectively. Although turnover frequencies (TOFs) are usually used to compare the catalytic activity, it is hard to determine the actual active sites (e.g., Pt, TiO_2, and the Pt-TiO_2 interface). Hence, we use TOF_M (mC_0/n_M) and the specific reaction rate (mC_0/w_M) to compare the catalytic activities (Table S2). Obviously, $Pt_{1.9\,nm}/TiO_2$ possesses a much higher TOF_{Pt} and specific reaction rate than $Pt_{1.3\,nm}/TiO_2$ and $Pt_{3.0\,nm}/TiO_2$. At 140 °C, TOF_{Pt} over $Pt_{1.3\,nm}/TiO_2$, $Pt_{1.9\,nm}/TiO_2$, and $Pt_{3.0\,nm}/TiO_2$ is 1.7×10^{-3}, 5.9×10^{-3}, and $3.2 \times 10^{-3}\,s^{-1}$, respectively. Fig. S2B shows the linear-fitting Arrhenius plots for complete toluene oxidation over the $Pt_{1.3\,nm}/TiO_2$, $Pt_{1.9\,nm}/TiO_2$, and $Pt_{3.0\,nm}/TiO_2$ catalysts, and the apparent activation energy (E_a) values are summarized in Table S2. Expectedly, $Pt_{1.9\,nm}/TiO_2$ (70.0 kJ/mol) possesses a lower E_a than $Pt_{1.3\,nm}/TiO_2$ (90.5 kJ/mol) and $Pt_{3.0\,nm}/TiO_2$ (82.9 kJ/mol).

To further explain the size effect on the catalytic activity of Pt/TiO_2 for toluene oxidation, we carry out TEM (Fig. S1), A C-H AADF-STEM (Fig. 1), XRD (Fig. S3), BET (Table S1), XPS (Fig. S4), and toluene-TPD (Fig. S5) characterization studies. The Pt NPs are well dispersed on the surface of the TiO_2 support. The surface area of the $Pt_{1.3\,nm}/TiO_2$, $Pt_{1.9\,nm}/TiO_2$, and $Pt_{3.0\,nm}/TiO_2$ catalysts is 30.7, 28.6, and 29.6 m^2/g, respectively. The microstructure of $Pt_{1.9\,nm}/TiO_2$ is well investigated via the HRTEM, HAADF-STEM, and EDS-mapping analyses (Fig. 1). The two lattice planes with spacings of 0.23 and 0.35 nm on the $Pt_{1.9\,nm}/TiO_2$ catalyst can be attributed to the Pt (111) and TiO_2 (101) planes

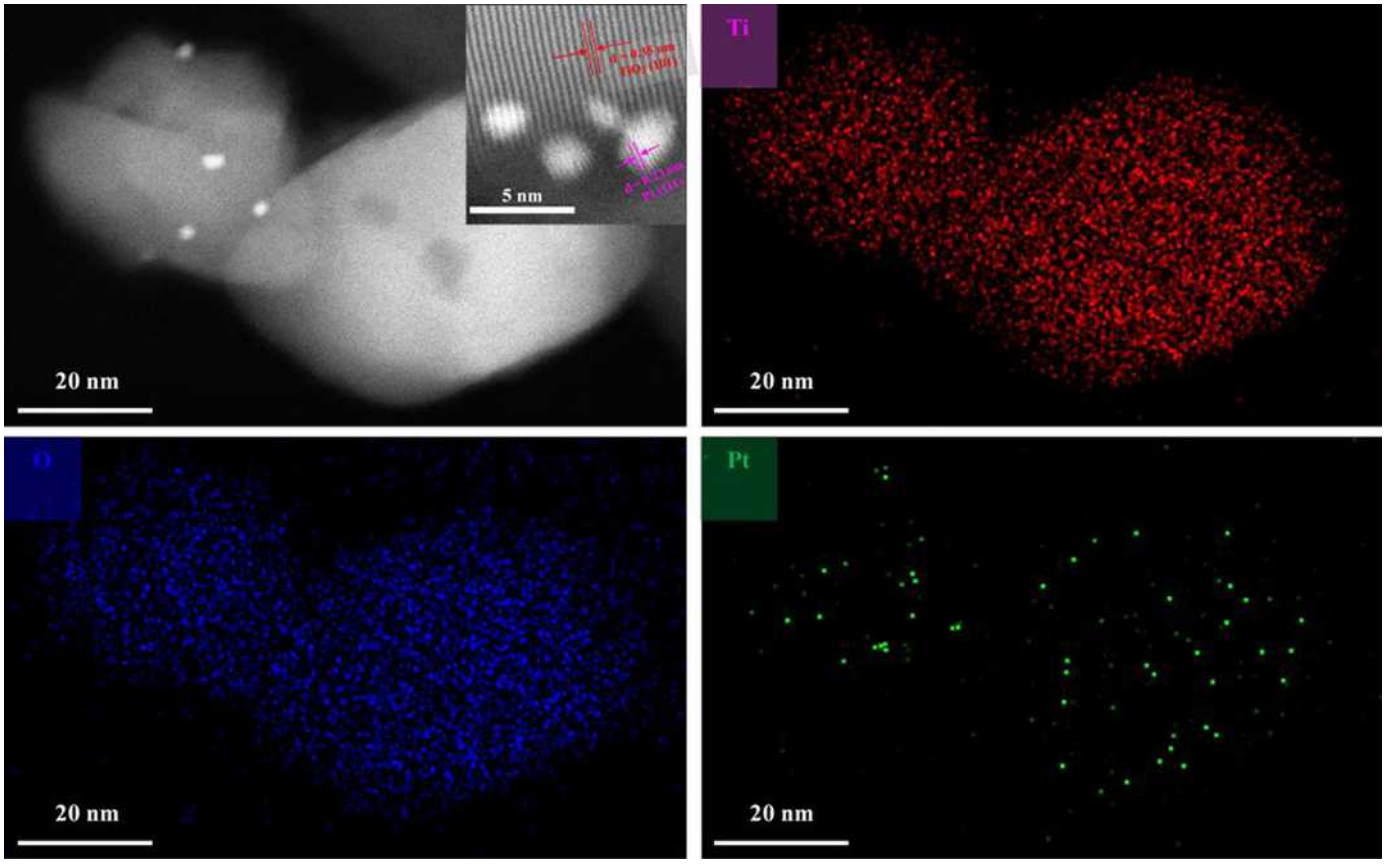

Fig. 1. HAADF-STEM and HRTEM images as well as element analysis mapping of the $Pt_{1.9\ nm}/TiO_2$ catalyst.

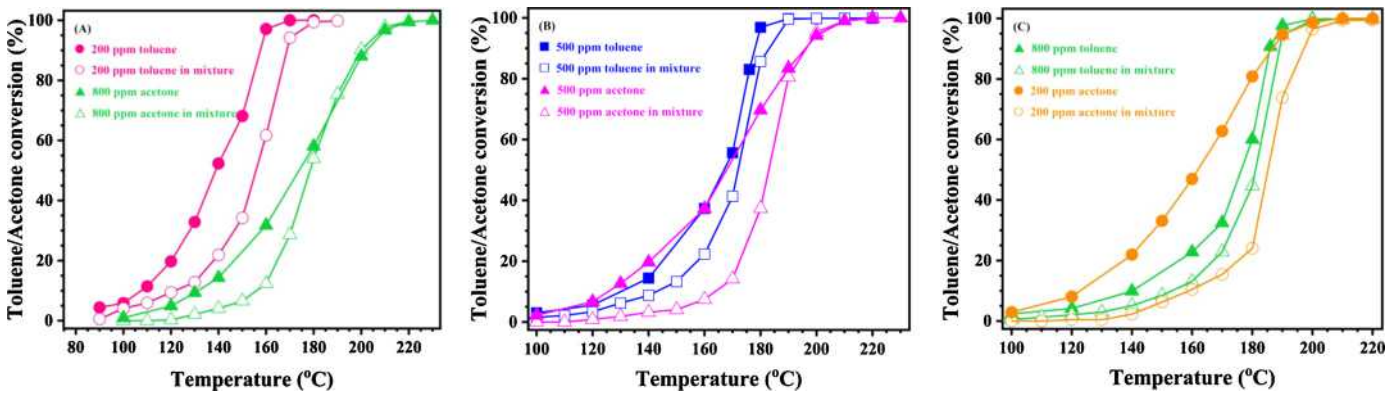

Fig. 2. Toluene and acetone conversion (alone and in mixture) as a function of temperature over the $Pt_{1.9\ nm}/TiO_2$ catalyst. Reaction conditions: x ppm toluene + y ppm acetone (x + y = 1000; x = 200, 500, and 800) + 20 vol% O_2 + N_2 balanced gas, and WHSV = 40,000 mL/(g h).

[49,50], respectively. From the HAADF-ATEM and EDS-mapping images, it can be further confirmed that Ti, O, and Pt elements are uniformly distributed on $Pt_{1.9\ nm}/TiO_2$. The higher catalytic activity of $Pt_{1.9\ nm}/TiO_2$ for complete toluene oxidation is associated with the larger amount of surface adsorbed oxygen species and better adsorption capacity of toluene. The detailed results and discussion are well described in the SI.

3.2. Catalytic activity of $Pt_{1.9\ nm}/TiO_2$ for (toluene + acetone) mixture oxidation

On one hand, $Pt_{1.9\ nm}/TiO_2$ exhibits a higher catalytic activity than $Pt_{1.3\ nm}/TiO_2$ and $Pt_{3.0\ nm}/TiO_2$ for toluene oxidation. On the other hand, aromatic hydrocarbons and ketones are the main compounds emitted in the concentrated areas of pharmaceutical companies. Therefore, we further investigate the catalytic activity of $Pt_{1.9\ nm}/TiO_2$ for (toluene + acetone) mixture oxidation. Under industrial conditions, the concentration of various VOCs in emissions would fluctuate depending on the working conditions. To better simulate the real emissions, the adopted reaction conditions are x ppm toluene + y ppm acetone (x + y = 1000; x = 200, 500, and 800) + 20 % O_2 + N_2 (balance gas), and a WHSV = 40,000 mL/(g h). Shown in Fig. 2 are the toluene and acetone conversion (alone and in a mixture) as a function of the temperature over the $Pt_{1.9\ nm}/TiO_2$ catalyst. It can be seen that there is a strong inhibiting effect on the catalytic activity of $Pt_{1.9\ nm}/TiO_2$ for (toluene + acetone) mixture oxidation, especially at a low reaction temperature. $T10$ % and $T50$ % for (toluene + acetone) mixture oxidation are higher than the corresponding $T10$ % and $T50$ % for single toluene or acetone oxidation (Fig. S6 and Table S3). Furthermore, the presence of toluene greatly inhibits the oxidation of acetone.

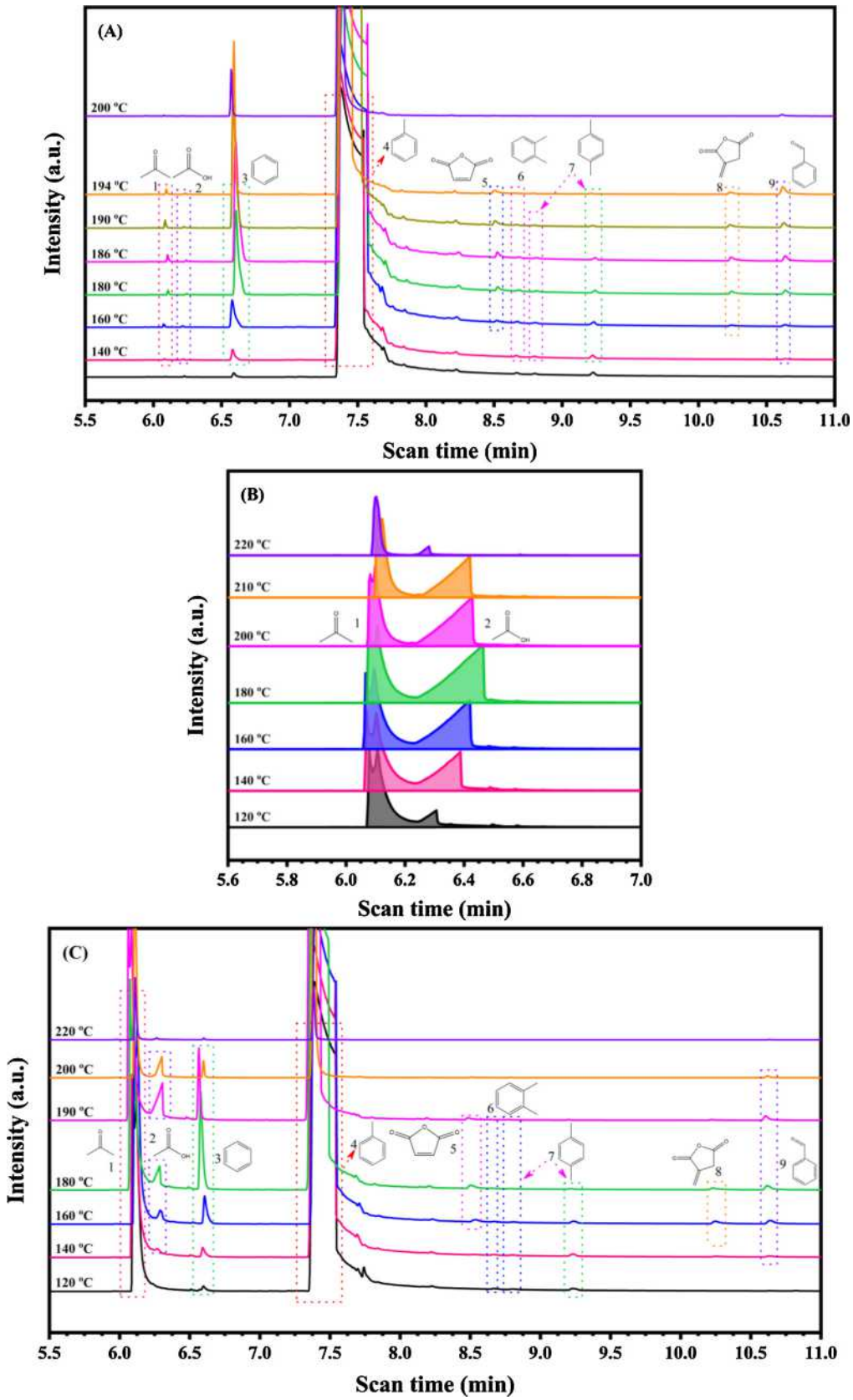

Fig. 3. Possible reaction intermediates detected during (A) toluene, (B) acetone, and (C) (toluene + acetone) mixture oxidation over $Pt_{1.9\ nm}/TiO_2$ at different temperature.

Table 1
Possible reaction intermediates detected by GC–MS during catalytic oxidation of VOCs over $Pt_{1.9\ nm}/TiO_2$.

Order	Molecular formula	Compound name	Molecular structure
1	C_3H_6O	acetone	
2	$C_2H_3O_2$	acetic acid	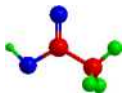
3	C_6H_6	benzene	
4	C_7H_8	toluene	
5	$C_4H_2O_3$	maleic anhydride	
6	C_8H_{10}	o-xylene	
7	C_8H_{10}	p-xylene	
8	$C_5H_4O_3$	itaconic anhydride	
9	C_7H_6O	benzaldehyde	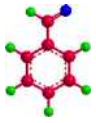

At a high reaction temperature, after toluene is completely removed, acetone could be rapidly oxidized, and the conversion curve of acetone in the mixture coincides with that of single acetone. Anyway, both toluene and acetone could be totally oxidized over $Pt_{1.9\ nm}/TiO_2$ at a temperature lower than 220 °C. It should be mentioned that although similar inhibiting phenomena was observed by Verykios and co-workers [42] for (benzene + butanol) mixture oxidation, the possible reasons need further explanation, as follows.

Shown in Fig. S7 is the toluene and acetone reaction rate normalized per gram of catalyst as a function of the temperature over the $Pt_{1.9\ nm}/TiO_2$ catalyst. Generally, the toluene and acetone reaction rate increases with a rise in the reaction temperature. At a reaction temperature less than 180 °C (Table S4), the toluene reaction rate for the complete oxidation of 200, 500, or 800 ppm toluene alone is higher than that for the complete oxidation of toluene with the corresponding concentration in the mixture. At a reaction temperature less than 190 °C (Table S5), the acetone reaction rate for the complete oxidation of 200, 500, or 800 ppm acetone alone is higher than that for the complete oxidation of acetone with the corresponding concentration in the mixture. However, at a reaction temperature larger than 200 °C, the toluene and acetone reaction rate for the complete oxidation of toluene and/or acetone alone or in the mixture does not exhibit much of a difference. Such results further confirm the mutual inhibition for the catalytic removal of a toluene and acetone mixture over the $Pt_{1.9\ nm}/TiO_2$ catalyst. We also compare the catalytic performance of the present $Pt_{1.9\ nm}/TiO_2$ catalyst and the supported noble metal catalysts reported in the literature, in terms of *T*50 % and *T*90 % (the corresponding temperature required for 50 % and 90 % conversion of toluene or acetone), the toluene or acetone reaction rate, and $TOF_{noble\ metal}$ (Tables 2 and 3). For the complete oxidation of toluene, the present $Pt_{1.9\ nm}/TiO_2$ catalyst exhibits a lower *T*90 %, a larger toluene reaction rate, and a higher $TOF_{noble\ metal}$ than the 0.3 wt% Pt/8.9 wt% Co_3O_4/Al_2O_3 [51], 1.4 wt% Pt/Al_2O_3 [51], 1.0 wt% Pt/MOR [52], 1.0 wt% Pt/Beta zeolite [53], 0.5 wt% Pt/Mn_2O_3 [54], 1.0 wt% Pt/Al_2O_3-CeO_2 [55], 0.93 wt% Pt/KIT-6 [56], and 0.74 wt% Au/Al_2O_3 [57] catalysts and a higher *T*90 %, a smaller toluene reaction rate and a lower $TOF_{noble\ metal}$ than the 0.24 wt% Pt/CeO_2 [58] catalyst. For the complete oxidation of acetone, the present $Pt_{1.9\ nm}/TiO_2$ catalyst exhibits a lower *T*90 %, a larger acetone reaction rate, and a higher $TOF_{noble\ metal}$ than the 1.0 wt% Pt-10 wt% Ce/Al_2O_3 [39], 1.0 wt% Pt-10 wt% Ce/TiO_2 [39], 1.0 wt% Pd/TiO_2 [59], 1.0 wt% Pd-20 wt% Mn/TiO_2 [59], 0.03 wt% Pd/γ-Al_2O_3 [60], 0.03 wt% $Pd/CeO_2/\gamma$-Al_2O_3 [60], and 0.05 wt% Pt/TiO_2 [61] catalysts. Obviously, the present $Pt_{1.9\ nm}/TiO_2$ catalyst exhibits a better catalytic performance than the counterparts in the literature.

3.3. Possible reaction intermediates for toluene, acetone, and the (toluene + acetone) mixture oxidation over $Pt_{1.9\ nm}/TiO_2$

To explain the inhibiting phenomena, we online detect the reaction intermediates obtained by oxidizing the 1000 ppm toluene, 1000 pm acetone, (500 ppm toluene +500 ppm acetone) mixture over $Pt_{1.9\ nm}/TiO_2$ at various reaction temperatures via the TD-GC/MS technique,

Table 2
*T*50 % and *T*90 %, toluene reaction rate, and $TOF_{noble\ metal}$ over various supported noble metal catalysts.

Order	Catalyst	Toluene concentration (ppm)	Space velocity (mL/(g h))	$T_{50\%}$ (°C)	$T_{90\%}$ (°C)	Reaction rate(μmol/(g_{cat} s)) at 160 °C	$TOF_{noble\ metal}$ ($\times 10^{-3}$ s^{-1}) at 160 °C	Reference
1	0.12 wt% $Pt_{1.9\ nm}/TiO_2$	1000	40,000	182	190	0.036[a]	5.915[a]	This work
2	0.3 wt% Pt/8.9 wt% Co_3O_4/Al_2O_3	1000	20,000	210	220	0.007	0.762	[51]
3	1.4 wt% Pt/Al_2O_3	1000	20,000	180	197	0.029	0.667	[51]
4	1.0 wt% Pt/MOR	1000	60,000	195	210	0.032	0.035	[52]
5	1.0 wt% Pt/Beta zeolite	1000	60,000	197	206	0.034	0.590	[53]
6	0.5 wt% Pt/Mn_2O_3	1000	40,000	208	240	0.027	1.210	[54]
7	1.0 wt% Pt/Al_2O_3-CeO_2	1000	8400	190	218	0.010	0.204	[55]
8	0.93 wt% Pt/KIT-6	500	80,000	180	196	0.032	0.106	[56]
9	0.74 wt% Au/Al_2O_3	1000	20,000	290	317	0.014[b]	0.375[b]	[57]
10	0.24 wt% Pt/CeO_2	1000	48,000	132	143	0.060[c]	6.750[c]	[58]

[a] Toluene reaction rate and $TOF_{noble\ metal}$ obtained at 140°C.
[b] Toluene reaction rate and $TOF_{noble\ metal}$ obtained at 230 °C.
[c] Toluene reaction rate and $TOF_{noble\ metal}$ obtained at 110 °C.

Table 3
*T*50 % and *T*90 %, acetone reaction rate, and $TOF_{noble\ metal}$ over various supported noble metal catalysts.

Order	Catalyst	Acetone concentration (ppm)	Space velocity (mL/(g h))	$T_{50\%}$ (°C)	$T_{90\%}$ (°C)	Reaction rate (μmol/(g_{cat} s)) at 180 °C	$TOF_{noble\ metal}$ ($\times 10^{-3}$ s^{-1}) at 180 °C	Reference
1	0.12 wt% $Pt_{1.9\ nm}/TiO_2$	1000	40,000	194	207	0.054[a]	8.781[a]	This work
2	1.0 wt% Pt-10 wt% Ce/Al_2O_3	1000	44,800	214	238	0.051	0.993	[39]
3	1.0 wt% Pt-10 wt% Ce/TiO_2	1000	44,800	210	236	0.046	0.893	[39]
4	1.0 wt% Pd/TiO_2	1000	30,000	257	295	0.007	0.073	[59]
5	1.0 wt% Pd-20 wt% Mn/TiO_2	1000	30,000	205	251	0.044	0.471	[59]
6	0.03 wt% $Pd/\gamma\text{-}Al_2O_3$	1000	40,000	206	215	0.002	0.725	[60]
7	0.03 wt% $Pd/CeO_2/\gamma\text{-}Al_2O_3$	1000	18,000	198	208	0.014	5.077	[60]
8	0.05 wt% Pt/TiO_2	1000	40,000	236	274	0.006[a]	2.280[a]	[61]

[a] Acetone reaction rate and $TOF_{noble\ metal}$ obtained at 140 °C.

and the results are shown in Fig. 3 and Table 1. For the complete oxidation of single toluene (Fig. 3A), 8 kinds of intermediates are observed. Benzene, *o*-xylene, *p*-xylene, and benzaldehyde are the main intermediates obtained by toluene oxidation at low reaction temperatures (< 140 °C). The formation of benzene and *p*-xylene can be ascribed to the disproportionate amount of toluene. The formation of *o*-xylene is assigned to the isomerization of *p*-xylene and benzene. The formation of benzaldehyde can be attributed to the partial oxidation of toluene. In addition, some small molecular substances (e.g., acetone and acetic acid) are also detected at low reaction temperatures (< 140 °C), which demonstrates the deep oxidation of little toluene. At a temperature higher than 160 °C, maleic anhydride and itaconic anhydride are found due to the cracking of the benzene ring. At 200 °C, most of the intermediates disappear due to the complete oxidation of toluene. For the complete oxidation of single acetone (Fig. 3B), only acetic acid is observed. The amount of acetic acid first gradually increases with a rise in the temperature and then decreases at a temperature higher than 200 °C. While the intermediates are detected for the complete oxidation of single toluene or acetone, no new intermediates are observed for the complete oxidation of the (toluene + acetone) mixture (Fig. 3C). Therefore, we roughly deduce that although the co-presence of toluene and acetone causes mutual inhibition, the catalytic oxidation mechanism of the (toluene + acetone) mixture does not change.

3.4. Adsorption and activation for toluene, acetone, and the (toluene + acetone) mixture over $Pt_{1.9\ nm}/TiO_2$

To further explain the inhibiting phenomena and investigate the catalytic mechanism, we carry out the VOC-TPD and VOC-TPO characterization methods to probe the adsorption and activation ability of $Pt_{1.9\ nm}/TiO_2$ for VOCs. The TPD and TPO profiles of toluene, acetone, and the (toluene + acetone) mixture over $Pt_{1.9\ nm}/TiO_2$ are shown in Fig. 4. From the toluene-TPD profiles (Fig. 4A), we detect a sharp toluene (m/z = 91) desorption peak at 77 °C and a strong H_2O (m/z = 18) desorption peak at 80 °C due to the physical desorption or weak chemisorption of toluene and H_2O, respectively. Due to the partial oxidation of the chemisorbed toluene, with a rise in the temperature, a very small benzene (m/z = 78) desorption peak appears at 420 °C, the two desorption peaks appear at 338–350 °C and 518–523 °C, which are attributed to CO (m/z = 28), CO_2 (m/z = 44), acetic acid (m/z = 45), and acetone (m/z = 43), and a H_2O desorption peak is observed at 338 °C. From the toluene-TPO profiles (Fig. 4B), the intensity of the toluene desorption peak at 73 °C greatly decreases, while that of the H_2O desorption peak at 75 °C is well maintained; the desorption temperature of CO, CO_2, acetic acid, and acetone in the toluene-TPO profile moves towards to significantly a lower temperature than that observed in the toluene-TPD profiles; the intensity of the CO_2 desorption peak greatly increases, while that of the CO desorption peak greatly decreases compared with that of the toluene-TPD profiles (Fig. 4A). Thus, the presence of O_2 benefits the activation and complete oxidation of toluene. From the acetone-TPD (Fig. 4C) and acetone-TPO (Fig. 4D) profiles, a similar conclusion could be obtained. In addition, note that the intensity of the acetone desorption peak at 82 °C is well maintained in the acetone-TPO profiles. The TPD (Fig. 4E and G) and TPO (Fig. 4F) profiles for the (toluene + acetone) mixture almost exhibit the same desorption characteristics as the desorption characteristics of the corresponding acetone-TPD and acetone-TPO profiles. The adsorption capacity for acetone is much stronger than that for toluene (Fig. 4G) due to the difference in the polarity of toluene and acetone molecules [45]. The co-presence of toluene and acetone greatly decreases the adsorption amount of toluene and acetone. Based on the results of the VOC-TPD and VOC-TPO characterization, we deduce that mutual inhibition occurs due to the decrease in the adsorption ability for toluene and acetone [62] and further confirm that the co-presence of toluene and acetone does not change the activation and oxidation process.

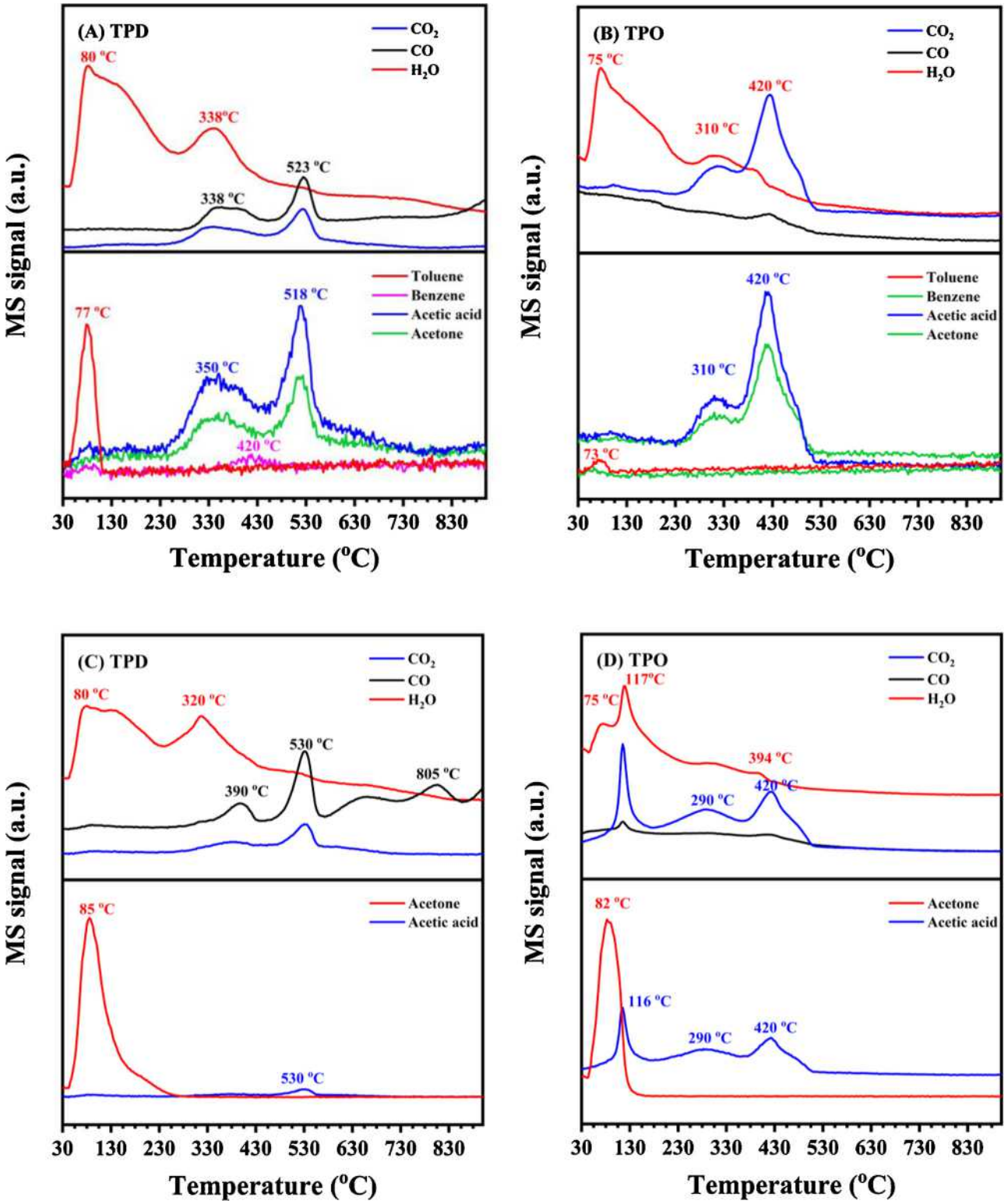

Fig. 4. Over $Pt_{1.9\ nm}/TiO_2$, TPD and TPO profiles of (A, B) toluene, (C, D) acetone, (E, F) (toluene + acetone) mixture; (G) TPD profiles of toluene and acetone (alone and in mixture).

3.5. In situ DRIFTS studies for the oxidation of toluene, acetone, and the (toluene + acetone) mixture over $Pt_{1.9\ nm}/TiO_2$

To further investigate the catalytic mechanism of the oxidation of toluene, acetone, and their mixture over the $Pt_{1.9\ nm}/TiO_2$ catalyst, we carry out the *in situ* DRIFTS experiments under the conditions of 1000 ppm toluene, 1000 ppm acetone, or (500 ppm toluene +500 ppm acetone) + 20 % O_2 + N_2 balance at 100, 160, 200, and 240 °C with different reaction times.

Shown in Fig. 5 are the *in situ* DRIFTS spectra obtained for the catalytic oxidation of toluene. Generally, the band at 3070 cm^{-1} belongs to the C—H stretching vibration ν(C—H) of the benzene ring. The band at 2973 cm^{-1} could be attributed to symmetric ν_s(C—H) stretching of the methyl group. The bands at 2931 and 2874 cm^{-1} are

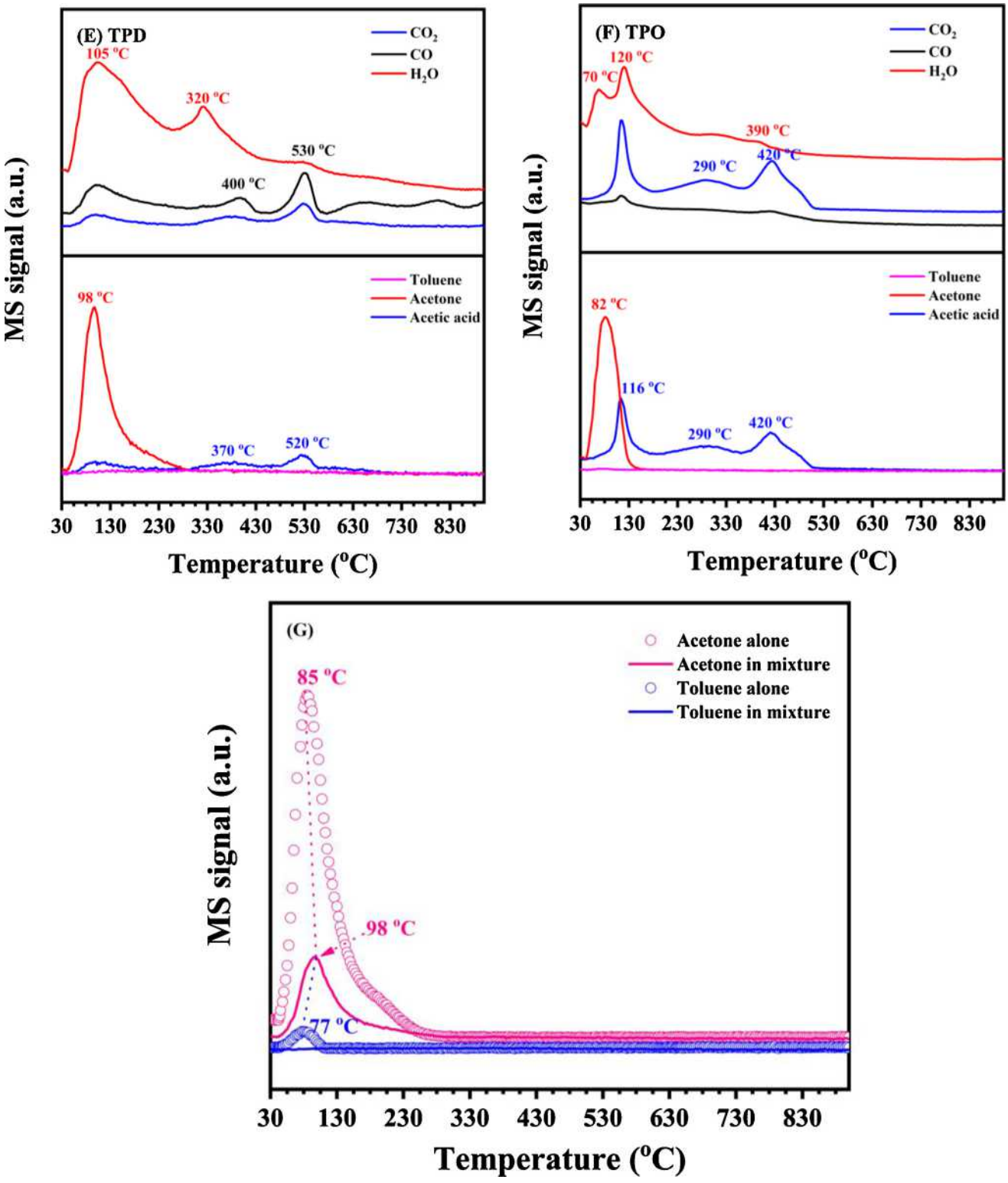

Fig. 4. (*continued*)

attributed to the asymmetric ν_{as}(C—H) and symmetric ν_s(C—H) stretching vibration of the methylene group, respectively. The bands at 1600 and 1495 cm^{-1} are assigned to the in-plane skeletal vibration of the benzene ring. The band at 1382 cm^{-1} is ascribed to the symmetric bending vibration of the methyl group. These bands are the characteristic signals of toluene molecules [63,64]. The intensity of the characteristic peaks of toluene gradually increases with an extension of time at 100 °C (Fig. 5A), indicating the effective adsorption of toluene on the surface of the $Pt_{1.9\ nm}/TiO_2$ catalyst, but gradually decreases with a rise in the temperature from 100 to 240 °C, demonstrating the effective removal of toluene over the $Pt_{1.9\ nm}/TiO_2$ catalyst. At 100–160 °C, some benzenoid rings, such as benzyl alcohol, benzaldehyde, and benzoate, are observed. The bands at 1771, 1512, 1453 and 1360 cm^{-1} indicate the formation of benzoate species [65,66]. The bands at 1578 and 1417 cm^{-1} belong to the stretching vibration of COO, further indicating the formation of benzyl acid [67]. The bands at

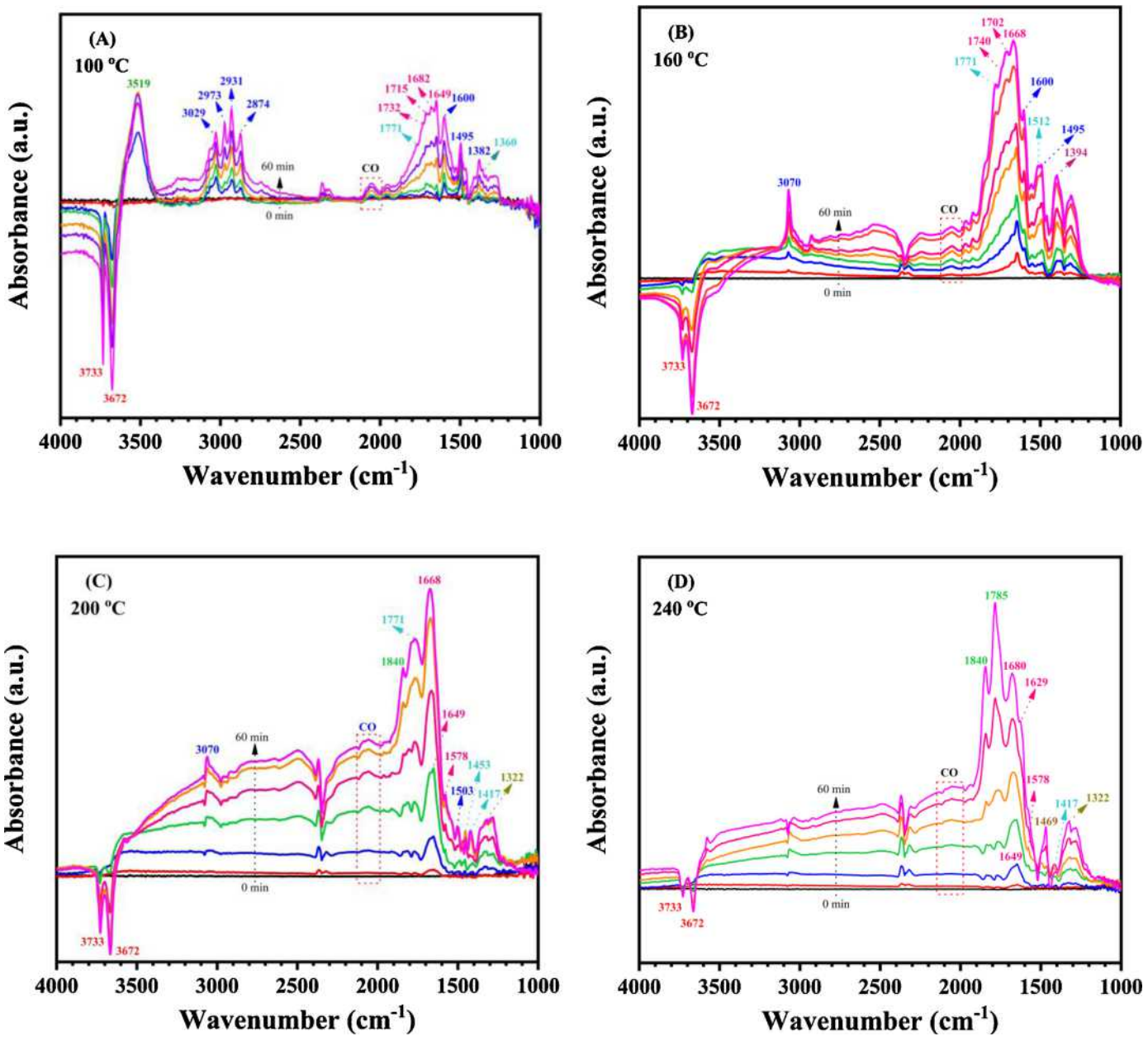

Fig. 5. *In-situ* DRIFTS spectra for the catalytic oxidation of toluene over $Pt_{1.9\ nm}/TiO_2$ at different reaction temperature and time.

1732, 1702, 1682, 1668, and 1649 cm^{-1} are ascribed to the symmetric stretching vibration of C═O (the typical bands of the aldehydic group) (Fig. 5B and C), suggesting the formation of benzaldehyde [65–70]. The bands at 1469 and 1322 cm^{-1}, which are due to the CH_2 deformation vibration of benzyl species, indicate the formation of benzyl alcohol. The bands at 1840 and 1785 cm^{-1}, which are due to the presence of small organic compounds (e.g., anhydrides), and the band at 1394 cm^{-1}, which is due to the stretching vibration and symmetric stretching of the carboxylate group, ν(OCO) (Fig. 5D), are observed, indicating the deep oxidation of toluene and the generation of acetate [66,71].

Shown in Fig. 6 are the *in situ* DRIFTS spectra obtained for the catalytic oxidation of acetone. Generally, the two negative sharp bands at 3733 and 3672 cm^{-1} are attributed to the stretching vibration of isolated and associated surface OH species on TiO_2 [72,73]. The bands at 2983, 2988, 2931, 2934, and 2874 cm^{-1} belong to the ν(C–H) stretching vibration of acetate species. The bands at 1700 and 1692 cm^{-1} could be assigned to the stretching vibration of C═O, and the band at 1369 cm^{-1} could be ascribed to the symmetrical deformation vibration of $-CH_3$ ($\delta_s(CH_3)$) in acetone molecules [72,74]. The sharp band at 1700 cm^{-1} quickly grows within 10 min. (Fig. 6A), further indicating the strong adsorption ability of $Pt_{1.9\ nm}/TiO_2$ for acetone. The band at 1590 cm^{-1} is due to bidentate carbonates [74]. The bands at 1552 [75] and 1400 cm^{-1} [76] are ascribed to the ν_a (COO) and CH bending vibration of the bidentate bridged HCOO (μ-formate) and formate species, respectively. The weak band at 2062 cm^{-1} is assigned to linear CO adsorbed on Pt. It is indicated that acetone could be partially oxidized, even at a low temperature. With a rise in the temperature from 160 to 240 °C (Fig. 6B–D), the bands at 1735, 1737, and 1718 cm^{-1} are observed due to the aliphatic carboxylate species [77]. The band at 1840 cm^{-1} belongs to the C═O stretching vibration of anhydride, suggesting the formation of acetic anhydrides. These results demonstrate the deep oxidation of acetone at high temperatures.

Shown in Fig. 7 are the *in situ* DRIFTS spectra obtained for the catalytic oxidation of the (toluene + acetone) mixture. At 100 °C, the

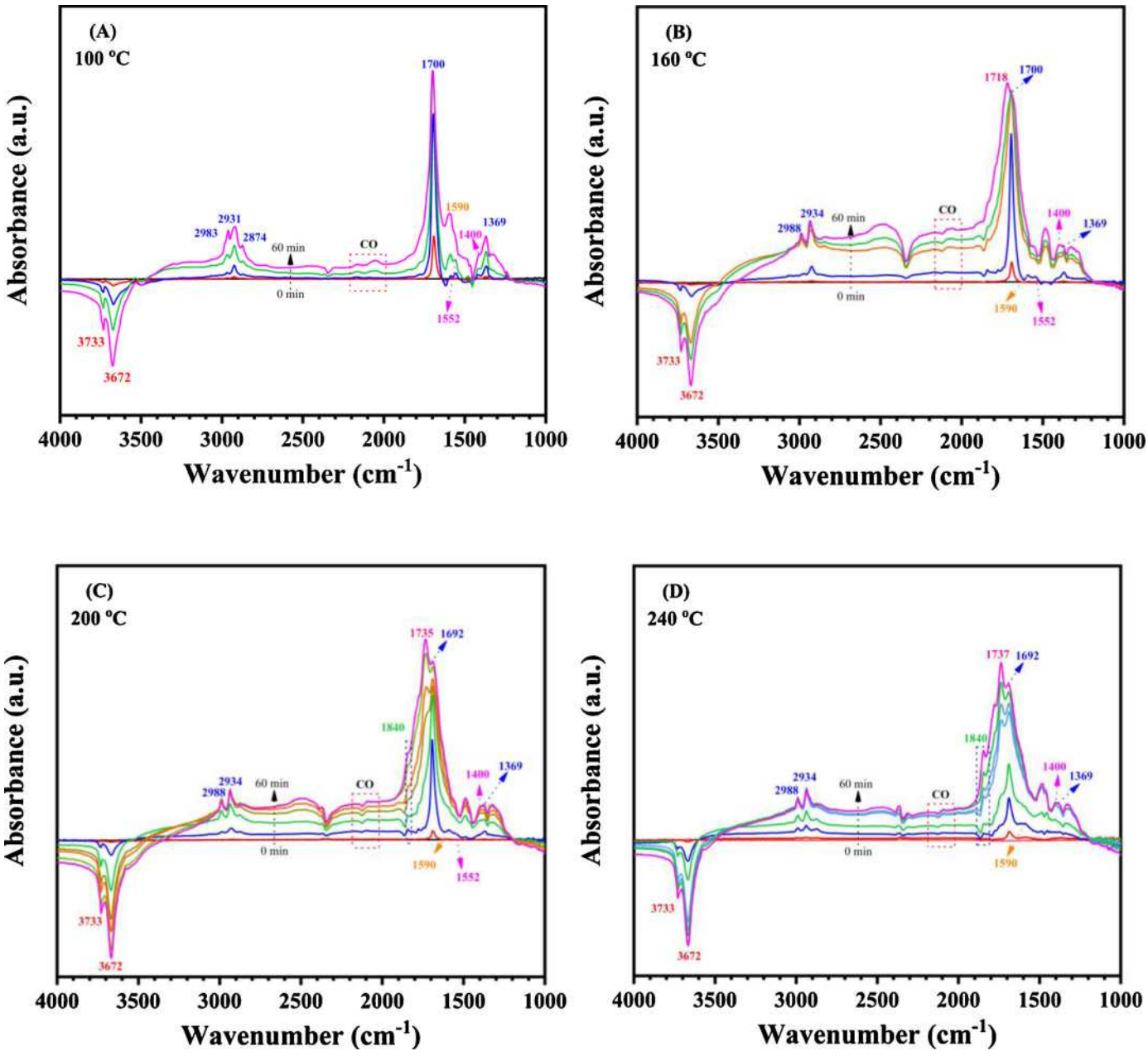

Fig. 6. *In-situ* DRIFTS spectra for the catalytic oxidation of acetone over $Pt_{1.9\ nm}/TiO_2$ at different reaction temperature and time.

spectra of the mixture (Fig. 7A) exhibit characteristics similar to those of the single acetone spectra (Fig. 6A), further confirming that the $Pt_{1.9\ nm}/TiO_2$ catalyst has a better adsorption capacity for acetone than for toluene (Fig. 4G). With a rise in the temperature from 160 to 200 °C (Fig. 7 and C), in addition to the characteristic bands observed for the oxidation of single acetone (Fig. 6), two bands observed for the oxidation of single toluene also appear at 1840 and 1788 cm^{-1} (Fig. 5D). Due to the co-presence of toluene and acetone, the band due to aliphatic carboxylates slightly shifts from 1737 to 1748 cm^{-1} at 240 °C (Fig. 7D). Generally, relative to the band observed for the oxidation of single toluene or acetone, no new bands are detected for the oxidation of the mixture. Therefore, we further confirm that the co-presence of toluene and acetone does not change the catalytic mechanism (Figs. 3 and 4).

3.6. Possible catalytic mechanism for the oxidation of toluene, acetone, and the (toluene + acetone) mixture over $Pt_{1.9\ nm}/TiO_2$

Based on the results obtained via the TD-GC/MS (Fig. 3), VOC-TPD and VOC-TPO (Fig. 4), and *in situ* DRIFTS (Figs. 5–7) techniques, we try to propose a possible catalytic mechanism for the oxidation of toluene and/or acetone over the $Pt_{1.9\ nm}/TiO_2$ catalyst. Scheme 1(A) shows the reaction pathway for the oxidation of toluene. Under the present reaction conditions, toluene is initially adsorbed on the active sites of the $Pt_{1.9\ nm}/TiO_2$ catalyst. Before the benzene ring opening reaction, two pathways might happen. During the first pathway, partially adsorbed toluene undergoes a disproportionation reaction to generate benzene and p-xylene, and p-xylene further undergoes an isomerization reaction to generate o-xylene. In the other pathway, the of adsorbed toluene is sequentially oxidized by the surface active oxygen to generate benzyl alcohol, benzaldehyde, and benzoic acid. With a rise in the reaction temperature, the benzene ring is cracked via further oxidation, forming itaconic anhydride, maleic anhydride, acetone, and acetic acid. Finally, the small molecular organic intermediates are totally oxidized into CO_2 and H_2O. Scheme 1(B) shows the reaction pathway for the oxidation of acetone. Acetone is adsorbed on the surface active sites and then reacted with the active oxygen to generate acetic acid and formic acid.

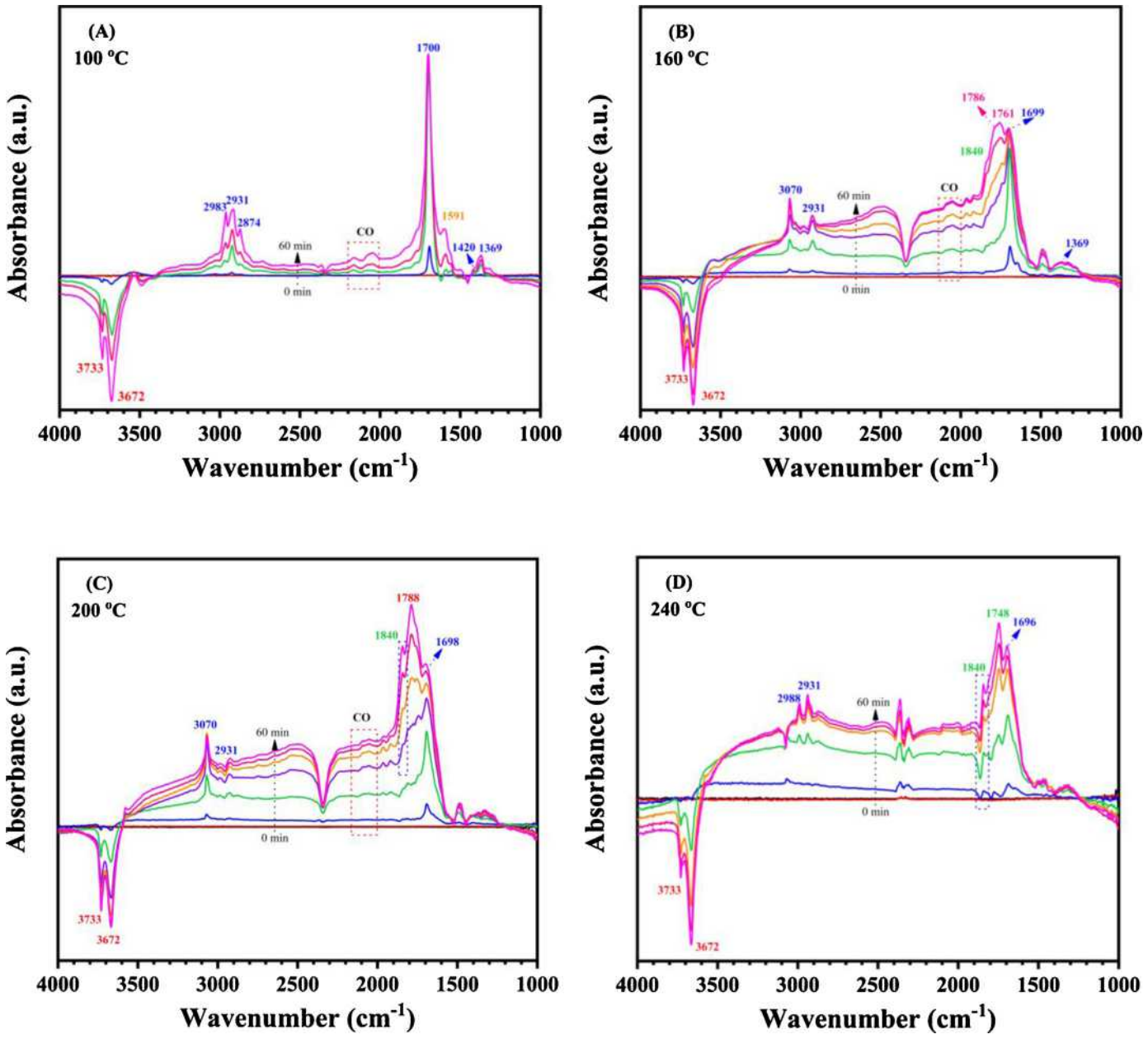

Fig. 7. *In-situ* DRIFTS spectra for the catalytic oxidation of (toluene + acetone) mixture over $Pt_{1.9\ nm}/TiO_2$ at different reaction temperature and time.

With a rise in the reaction temperature, acetic acid and formic acid are oxidized to bidentate carbonates species and then decomposed to CO_2 and H_2O. As mentioned above, the co-presence of toluene and acetone does not change the catalytic mechanism. Therefore, the reaction pathway for the oxidative removal of toluene and acetone in the mixture might follow Scheme 1(A) and (B), respectively.

3.7. Catalytic stability and H_2O and CO_2 tolerance of $Pt_{1.9\ nm}/TiO_2$ for the oxidation of the (toluene + acetone) mixture

For practical applications, the catalytic stability and H_2O and CO_2 tolerance are very important. Therefore, we further investigate the catalytic stability and H_2O and CO_2 tolerance of $Pt_{1.9\ nm}/TiO_2$ for the oxidation of a (500 ppm toluene + 500 ppm acetone) mixture. Within an on-stream reaction time of 30 h, toluene and acetone conversion remains unchanged at 200 °C (Fig. 8A) while at 184 °C, toluene conversion slightly decreases from 95 to 93 %, and acetone conversion decreases from 63 to 57 % (Fig. 8B). The slight decrease in the conversion is due to the accumulation of intermediates. As shown in Fig. 3C, benzaldehyde, benzene, maleic anhydride, and acetate are detected at 180 and 190 °C. Such species might occupy the active sites and then inhibit the deep oxidation of toluene and acetone [78]. Within a 25 h on-stream reaction time, the introduction of 5–10 vol% H_2O or CO_2 at 200 °C does not decrease toluene conversion but slightly decreases acetone conversion (Fig. 8C and E); at 184 °C, toluene conversion, especially acetone conversion, greatly decreases due to the addition of 5–10 vol% H_2O or CO_2 (Fig. 8D and F). Note that toluene and acetone conversion could be restored after cutting off H_2O or CO_2. The decrease in the catalytic activity of $Pt_{1.9\ nm}/TiO_2$, which is due to the co-presence of H_2O or CO_2, might be associated with the competitive adsorption of toluene, acetone, H_2O, and CO_2 on the active sites [79]. In addition, since the adsorption capacity of $Pt_{1.9\ nm}/TiO_2$ for acetone is much stronger than that for toluene, and the co-presence of toluene and acetone greatly decreases their adsorption amount (Fig. 4G), it is understandable that the negative effects are greater on acetone conversion than on toluene conversion (Fig. 8C–F).

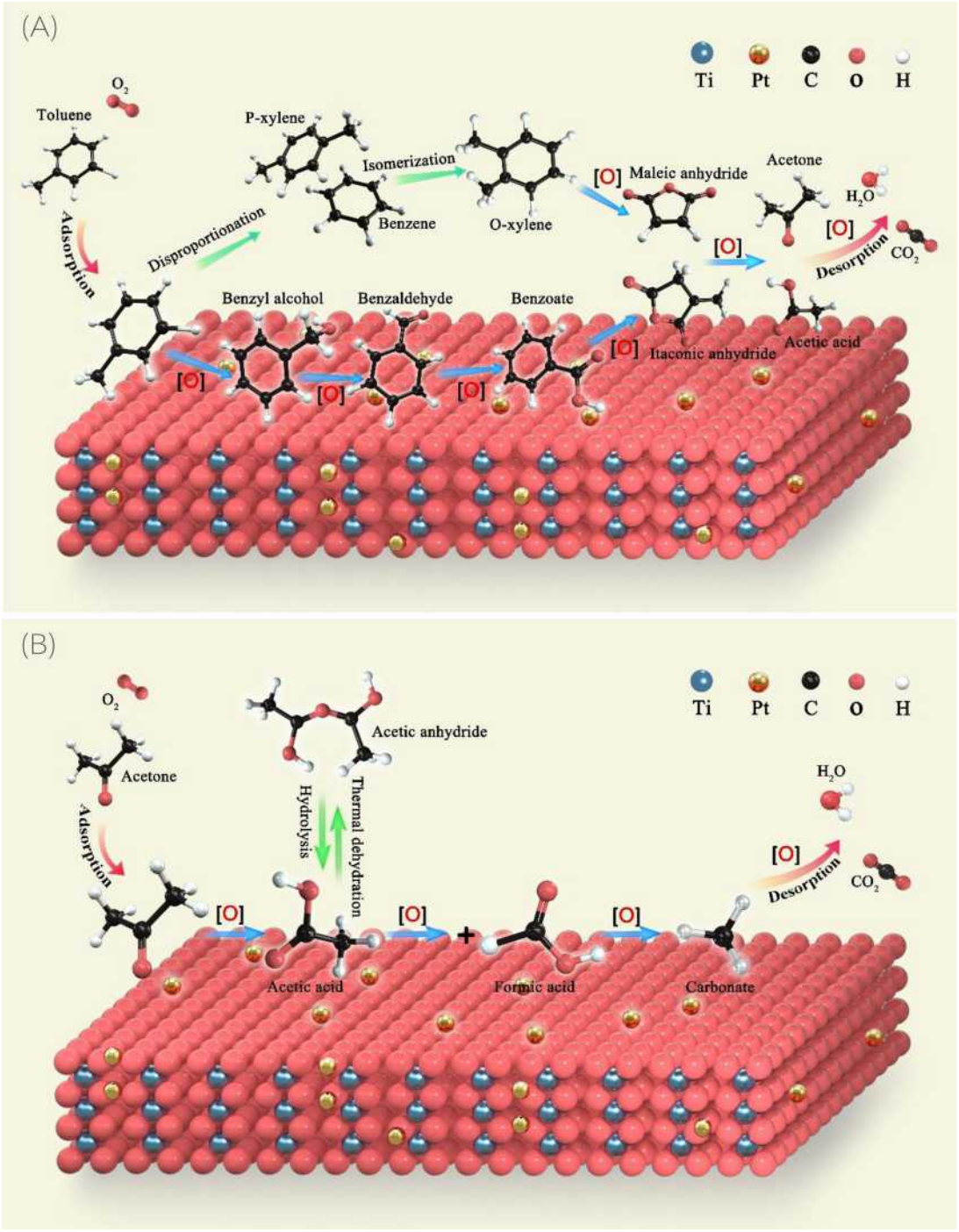

Scheme 1. Possible catalytic mechanism for the complete oxidation of (A) toluene and (B) acetone over the $Pt_{1.9\ nm}/TiO_2$ catalyst.

4. Conclusions

In the present study, we prepare a number of TiO_2 nanosheet-supported Pt nanocatalysts with an average size of 1.3, 1.9, and 3.0 nm. The surface area of the $Pt_{1.3\ nm}/TiO_2$, $Pt_{1.9\ nm}/TiO_2$, and $Pt_{3.0\ nm}/TiO_2$ catalysts is 30.7, 28.6, and 29.6 m^2/g, respectively. The as-obtained Pt/TiO_2 nanocatalysts exhibit size effects for the oxidation of toluene, and the higher catalytic activity of $Pt_{1.9\ nm}/TiO_2$ is associated with the larger amount of surface adsorbed oxygen species and better adsorption capacity of toluene. There is a strong inhibiting effect on the catalytic activity of $Pt_{1.9\ nm}/TiO_2$ for oxidizing the (toluene + acetone) mixture. In particular, the presence of toluene greatly inhibits the oxidation of acetone. From the VOC-TPD and VOC-TPO results, we deduce that mutual inhibition is due to the decrease in the adsorption ability of $Pt_{1.9\ nm}/TiO_2$ for toluene and acetone. Several intermediates, including benzene, o-xylene, p-xylene, benzaldehyde, maleic anhydride, itaconic anhydride, and acetic acid, are observed. We propose that over $Pt_{1.9\ nm}/TiO_2$, the co-presence of toluene and acetone does not change the catalytic mechanism, and the reaction pathway of the oxidative removal of toluene and acetone in the mixture might follow that of the oxidation of single toluene or acetone. $Pt_{1.9\ nm}/TiO_2$ exhibits a good catalytic activity and stability, as well as an H_2O and CO_2 tolerance. Both toluene and acetone could be totally oxidized over $Pt_{1.9\ nm}/TiO_2$ at a temperature lower than 220 °C. At 200 °C within a 25–30 h on-stream reaction time, toluene conversion remains unchanged, and acetone conversion only slightly decreases, even in the presence of 5–10 vol% H_2O

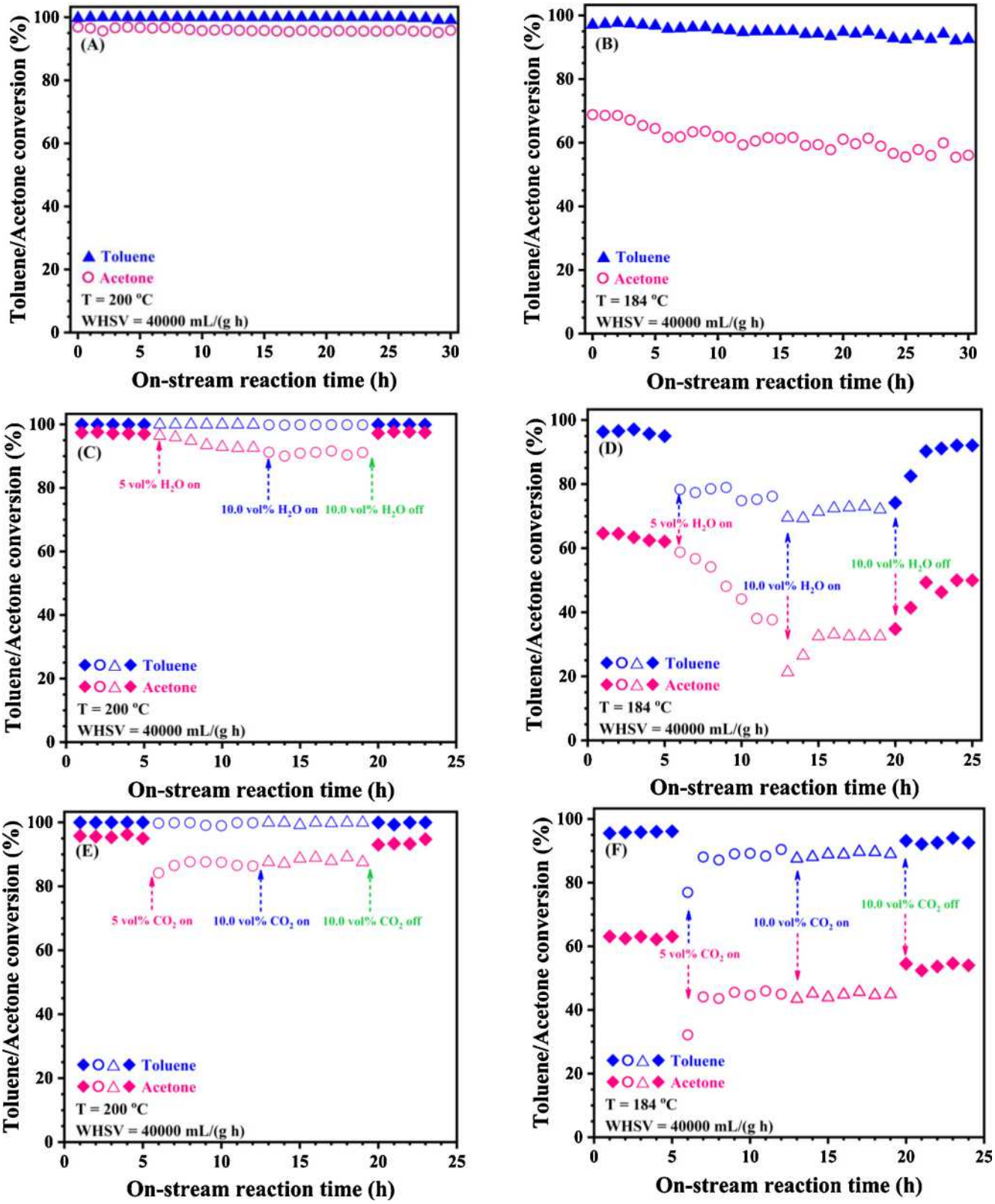

Fig. 8. (A, B) Catalytic stability and effect of (C, D) H_2O and (E, F) CO_2 on the catalytic activity of $Pt_{1.9\ nm}/TiO_2$ for the complete oxidation of (toluene + acetone) mixture.

or CO_2.

Credit author statement

Zhiwei Wang carried out experiments, wrote and modified the manuscript.

Peijie Ma and Kun Zheng performed and analyzed the TEM and AC–HAADF-STEM experiments.

Can Wang analyzed the experimental results.

Yuxi Liu analyzed the experimental results.

Hongxing Dai analyzed the experimental results.

Chongchen Wang analyzed the experimental results.

Hsing-Cheng Hsi analyzed the experimental results.

Jiguang Deng designed the experiments, analyzed the experimental results, wrote and modified the manuscript.

Declaration of Competing Interest

We certify that this manuscript consists of original, unpublished work which is not under consideration for publication elsewhere. We declare no competing financial interest.

Acknowledgements

This work is supported by the Natural Science Foundation of China (21622701, 21961160743, and U1507108) and National Key R&D Program of China (2016YFC0204800).

Appendix A. Supplementary data

Supplementary material related to this article can be found, in the online version, at doi:https://doi.org/10.1016/j.apcatb.2020.118963.

References

[1] Z.X. Zhang, Z. Jiang, W.F. Shangguan, Low-temperature catalysis for VOCs removal in technology and application: a state-of-the-art review, Catal. Today 264 (2016) 270–278.
[2] J.P. Tian, Q.P. Guo, Y. Chen, X. Li, H. Shi, L.J. Chen, Study on industrial metabolism of carbon in a Chinese fine chemical industrial park, Environ. Sci. Technol. 47 (2013) 1048–1056.
[3] A. Russell, A focus on particulate matter and health, Environ. Sci. Technol. 43 (2009) 4620–4625.
[4] C.Y. Hsu, H.C. Chiang, R.H. Shie, C.H. Ku, T.Y. Lin, M.J. Chen, N.T. Chen, Y.C. Chen, Ambient VOCs in residential areas near a large-scale petrochemical complex: spatiotemporal variation, source apportionment and health risk, Environ. Pollut. 240 (2018) 95–104.
[5] X.Y. Zhang, B. Gao, A.E. Creamer, C.C. Cao, Y.C. Li, Adsorption of VOCs onto engineered carbon materials: a review, J. Hazard. Mater. 338 (2017) 102–123.
[6] C.T. Yang, G. Miao, Y.H. Pi, Q.B. Xia, J.L. Wu, Z. Li, J. Xiao, Abatement of various types of VOCs by adsorption/catalytic oxidation: a review, Chem. Eng. J. 370 (2019) 1128–1153.
[7] J.H. Chen, X.N. Yu, X.C. Zhu, C.H. Zheng, X. Gao, K.F. Cen, Electrospinning synthesis of vanadium-TiO_2-carbon composite nanofibrous membranes as effective catalysts for the complete oxidation of low-concentration acetone, Appl. Catal. A Gen. 507 (2015) 99–108.
[8] J. Wan, P. Yang, X.L. Guo, R.X. Zhou, Elimination of 1,2-dichloroethane over (Ce, Cr)$_x$O$_2$/Nb_2O_5 catalysts: synergistic performance between oxidizing ability and acidity, Chin. J. Catal. 40 (2019) 1100–1108.
[9] J.J. Li, E.Q. Yu, S.C. Cai, X. Chen, J. Chen, H.P. Jia, Y.J. Xu, Noble metal free, CeO_2/$LaMnO_3$ hybrid achieving efficient photo-thermal catalytic decomposition of volatile organic compounds under IR light, Appl. Catal. B: Environ. 240 (2019) 141–152.
[10] H.L. Ye, Y.Q. Liu, S. Chen, H.Q. Wang, Z. Liu, Z.B. Wu, Synergetic effect between non-thermal plasma and photocatalytic oxidation on the degradation of gas-phase toluene: role of ozone, Chin. J. Catal. 40 (2019) 681–690.
[11] Z. Cheng, J.R. Li, P. Yang, S.F. Zuo, Preparation of MnCo/MCM-41 catalysts with high performance for chlorobenzene combustion, Chin. J. Catal. 39 (2018) 849–856.
[12] O.S.G.P. Soares, R.P. Rocha, J.J.M. Orfao, M.F.R. Pereira, J.L. Figueiredo, Ethyl and butyl acetate oxidation over manganese oxides, Chin. J. Catal. 39 (2018) 27–36.
[13] J. Ji, X.L. Lu, C. Chen, M. He, H.B. Huang, Potassium-modulated δ-MnO_2 as robust catalysts for formaldehyde oxidation at room temperature, Appl. Catal. B: Environ. 260 (2020) 118210.
[14] K. Vikrant, C.M. Park, K.H. Kim, S. Kumard, E.C. Jeon, Recent advancements in photocatalyst-based platforms for the destruction of gaseous benzene: performance evaluation of different modes of photocatalytic operations and against adsorption techniques, J. Photochem. Photobiol. C 41 (2019) 100316.
[15] K. Vikrant, K.H. Kim, A. Deep, Photocatalytic mineralization of hydrogen sulfide as a dual-phase technique for hydrogen production and environmental remediation, Appl. Catal. B: Environ. 259 (2019) 118025.
[16] N. Raza, W. Raza, H. Gul, M. Azam, J. Lee, K. Vikrant, K.H. Kim, Solar-light-active silver phosphate/titanium dioxide/silica heterostructures for photocatalytic removal of organic dye, J. Clean. Prod. 254 (2020) 120031.
[17] H. Anwer, A. Mahmood, J. Lee, K.H. Kim, J.W. Park, A.C.K. Yip, Photocatalysts for degradation of dyes in industrial effluents: opportunities and challenges, Nano Res. 12 (2019) 955–972.
[18] H. Anwer, J.W. Park, Synthesis and characterization of a heterojunction rGO/ZrO_2/Ag_3PO_4 nanocomposite for degradation of organic contaminants, J. Hazard. Mater. 358 (2018) 416–426.
[19] M.S. Kamal, S.A. Razzak, M.M. Hossain, Catalytic oxidation of volatile organic compounds (VOCs) − a review, Atmos. Environ. 140 (2016) 117–134.
[20] C. He, J. Cheng, X. Zhang, M. Douthwaite, S. Pattisson, Z.P. Hao, Recent advances in the catalytic oxidation of volatile organic compounds: a review based on pollutant sorts and sources, Chem. Rev. 119 (2019) 4471–4568.
[21] T. Gan, X.F. Chu, H. Qi, W.X. Zhang, Y.C. Zou, W.F. Yan, G. Liu, Pt/Al_2O_3 with ultralow Pt-loading catalyze toluene oxidation: promotional synergistic effect of Pt nanoparticles and Al_2O_3 support, Appl. Catal. B: Environ. 257 (2019) 117943.
[22] H.Y. Zhang, S.H. Sui, X.M. Zheng, R.R. Cao, P.Y. Zhang, One-pot synthesis of atomically dispersed Pt on MnO_2 for efficient catalytic decomposition of toluene at low temperatures, Appl. Catal. B: Environ. 257 (2019) 117878.
[23] S.S. Zhang, W.H. Pu, A.Y. Chen, Y.K. Xu, Y.Y. Wang, C.Z. Yang, J.Y. Gong, Oxygen vacancies enhanced photocatalytic activity towards VOCs oxidation over Pt deposited Bi_2WO_6 under visible light, J. Hazard. Mater. 384 (2020) 121478.
[24] G.Z. Liu, Y.J. Tian, B.F. Zhang, L. Wang, X.W. Zhang, Catalytic combustion of VOC on sandwich-structured Pt@ZSM-5 nanosheets prepared by controllable intercalation, J. Hazard. Mater. 367 (2019) 568–576.
[25] Z. Xu, H.M. Zhang, H.X. Zhong, Q.H. Lu, Y.F. Wang, D.S. Su, Effect of particle size on the activity and durability of the Pt/C electrocatalyst for proton exchange membrane fuel cells, Appl. Catal. B: Environ. 111−112 (2012) 264–270.
[26] K. Shinozaki, Y. Morimoto, B.S. Pivovar, S.S. Kocha, Re-examination of the Pt particle size effect on the oxygen reduction reaction for ultrathin uniform Pt/C catalyst layers without influence from Nafion, Electrochim. Acta 213 (2016) 783–790.
[27] H. Yano, M. Watanabe, A. Iiyama, H. Uchida, Particle-size effect of Pt cathode catalysts on durability in fuel cells, Nano Energy 29 (2016) 323–333.
[28] J. Perez, V.A. Paganin, E. Antolini, Particle size effect for ethanol electro-oxidation on Pt/C catalysts in half-cell and in a single direct ethanol fuel cell, J. Electroanal. Chem. 654 (2011) 108–115.
[29] S.Q. Song, K. Wang, Y.H. Liu, C.X. He, Y.R. Liang, R.W. Fu, D.C. Wu, Y. Wang, Highly ordered mesoporous carbons as the support for Pt catalysts towards alcohol electrooxidation: the combined effect of pore size and electrical conductivity, Int. J. Hydrogen Energy 38 (2013) 1405–1412.
[30] C.C. Ting, C.H. Chao, C.Y. Tsai, I.K. Cheng, F.M. Pan, Electrocatalytic performance of Pt nanoparticles sputter-deposited on indium tin oxide toward methanol oxidation reaction: the particle size effect, Appl. Surf. Sci. 416 (2017) 365–370.
[31] Y.Q. Zhu, T. Wang, T. Xu, Y.X. Li, C.Y. Wang, Size effect of Pt co-catalyst on photocatalytic efficiency of g-C_3N_4 for hydrogen evolution, Appl. Surf. Sci. 464 (2019) 36–42.
[32] J. Xing, Y.H. Li, H.B. Jiang, Y. Wang, H.G. Yang, The size and valence state effect of Pt on photocatalytic H_2 evolution over platinized TiO_2 photocatalyst, Int. J. Hydrogen Energy 39 (2014) 1237–1242.
[33] Y.X. Tuo, L.J. Shi, H.Y. Cheng, Y.A. Zhu, M.L. Yang, J. Xu, Y.F. Han, P. Li, W.K. Yuan, Insight into the support effect on the particle size effect of Pt/C catalysts in dehydrogenation, J. Catal. 360 (2018) 175–186.
[34] K. Kon, S.M.A.H. Siddiki, K.I. Shimizu, Size- and support-dependent Pt nanocluster catalysis for oxidant-free dehydrogenation of alcohols, J. Catal. 304 (2013) 63–71.
[35] V.V. Pushkarev, K. An, S. Alayoglu, S.K. Beaumont, G.A. Somorjai, Hydrogenation of benzene and toluene over size controlled Pt/SBA-15 catalysts: elucidation of the Pt particle size effect on reaction kinetics, J. Catal. 292 (2012) 64–72.
[36] B. Guo, Y. Song, G.L. Lv, A.L. Ren, Z. Du, F.H. He, X.H. Yin, Pollution analysis and health risk assessment of volatile organic compounds from dense pharmaceutical production areas, Environ. Chem. 33 (2014) 1354–1360.
[37] J.P. Zhong, Y.K. Zeng, D.D. Chen, S.P. Mo, M.Y. Zhang, M.L. Fu, J.L. Wu, Z.X. Su, P.R. Chen, D.Q. Ye, Toluene oxidation over Co^{3+}-rich spinel Co_3O_4: evaluation of chemical and by-product species identified by in situ DRIFTS combined with PTR-TOF-MS, J. Hazard. Mater. 386 (2020) 121957.
[38] X.Y. Wang, J.C. Zuo, Y.J. Luo, L.L. Jiang, New route to CeO_2/$LaCoO_3$ with high oxygen mobility for total benzene oxidation, Appl. Surf. Sci. 396 (2017) 95–101.
[39] Y.L. Ge, K.X. Fu, Q. Zhao, N. Ji, C.F. Song, D.G. Ma, Q.L. Liu, Performance study of modified Pt catalysts for the complete oxidation of acetone, Chem. Eng. Sci. 206 (2019) 499–506.
[40] K. Shimura, T. Fujitani, Effects of promoters on the performance of a VO_x/SiO_2 catalyst for the oxidation of methane to formaldehyde, Appl. Catal. A Gen. 577 (2019) 44–51.
[41] R. Beauchet, J. Mijoin, I. Batonneau-Gener, P. Magnoux, Catalytic oxidation of VOCs on NaX zeolite: mixture effect with isopropanol and o-xylene, Appl. Catal. B: Environ. 100 (2010) 91–96.
[42] P. Papaefthimiou, T. Ioannides, X.E. Verykios, Combustion of non-halogenated volatile organic compounds over group VIII metal catalysts, Appl. Catal. B: Environ. 13 (1997) 175–184.

[43] P. Papaefthimiou, T. Ioannides, X.E. Verykios, Performance of doped Pt/TiO_2 (W^{6+}) catalysts for combustion of volatile organic compounds (VOCs), Appl. Catal. B: Environ. 15 (1998) 75–92.
[44] S. Ordóñez, L. Bello, H. Sastre, R. Rosal, F.V. Diez, Kinetics of the deep oxidation of benzene, toluene, n-hexane and their binary mixtures over a platinum on γ-alumina catalyst, Appl. Catal. B: Environ. 38 (2002) 139–149.
[45] C. He, P. Li, J. Cheng, Z.P. Hao, Z.P. Xu, A comprehensive study of deep catalytic oxidation of benzene, toluene, ethyl acetate, and their mixtures over Pd/ZSM-5 catalyst: mutual effects and kinetics, Water Air Soil Pollut. 209 (2010) 365–376.
[46] M. Chen, J.Z. Ma, B. Zhang, F. Wang, Y.B. Li, C.B. Zhang, H. He, Facet-dependent performance of anatase TiO_2 for photocatalytic oxidation of gaseous ammonia, Appl. Catal. B: Environ. 223 (2018) 209–215.
[47] W.D. Michalak, J.M. Krier, K. Komvopoulos, G.A. Somorjai, Structure sensitivity in Pt nanoparticle catalysts for hydrogenation of 1,3-butadiene: in situ study of reaction intermediates using SFG vibrational spectroscopy, J. Phys. Chem. C 117 (2013) 1809–1817.
[48] R.M. Rioux, H. Song, J.D. Hoefelmeyer, P.D. Yang, G.A. Somorjai, High-surface-area catalyst design: synthesis, characterization, and reaction studies of platinum nanoparticles in mesoporous SBA-15 silica, J. Phys. Chem. B 109 (2005) 2192–2202.
[49] J. Chen, M.G. Wang, J. Han, R. Guo, TiO_2 nanosheet/NiO nanorod hierarchical nanostructures: p-n heterojunctions towards efficient photocatalysis, J. Colloid Interface Sci. 562 (2020) 313–321.
[50] R.S. Peng, X.B. Sun, S.J. Li, L.M. Chen, M.L. Fu, J.L. Wu, D.Q. Ye, Shape effect of Pt/CeO_2 catalysts on the catalytic oxidation of toluene, Chem. Eng. J. 306 (2016) 1234–1246.
[51] H.G. Yang, J.G. Deng, Y.X. Liu, S.H. Xie, P. Xu, H.X. Dai, Pt/Co_3O_4/3DOM Al_2O_3: highly effective catalysts for toluene combustion, Chin. J. Catal. 37 (2016) 934–946.
[52] J.Y. Zhang, C. Rao, H.G. Peng, C. Peng, L. Zhang, X.L. Xu, W.M. Liu, Z. Wang, N. Zhang, X. Wang, Enhanced toluene combustion performance over Pt loaded hierarchical porous MOR zeolite, Chem. Eng. J. 334 (2018) 10–18.
[53] C.Y. Chen, J. Zhu, F. Chen, X.J. Meng, X.M. Zheng, X.H. Gao, F.S. Xiao, Enhanced performance in catalytic combustion of toluene over mesoporous beta zeolite-supported platinum catalyst, Appl. Catal. B: Environ. 140 – 141 (2013) 199–205.
[54] W.B. Pei, Y.X. Liu, J.G. Deng, K.F. Zhang, Z.Q. Hou, X.T. Zhao, H.X. Dai, Partially embedding Pt nanoparticles in the skeleton of 3DOM Mn_2O_3: an effective strategy for enhancing catalytic stability in toluene combustion, Appl. Catal. B: Environ. 256 (2019) 117814.
[55] Z. Abbasi, M. Haghighi, E. Fatehifar, S. Saedy, Synthesis and physicochemical characterizations of nanostructured Pt/Al_2O_3-CeO_2 catalysts for total oxidation of VOCs, J. Hazard. Mater. 186 (2011) 1445–1454.
[56] D.Y. Yang, S.Y. Fu, S.S. Huang, W. Deng, Y. Wang, L.M. Guo, T. Ishihara, The preparation of hierarchical Pt/ZSM-5 catalysts and their performance for toluene catalytic combustion, Microporous Mesoporous Mater. 296 (2020) 109802.
[57] H.G. Yang, J.G. Deng, Y.X. Liu, S.H. Xie, Z.X. Wu, H.X. Dai, Preparation and catalytic performance of Ag, Au, Pd or Pt nanoparticles supported on 3DOM CeO_2-Al_2O_3 for toluene oxidation, J. Mol. Catal. A Chem. 414 (2016) 9–18.
[58] R.S. Peng, S.J. Li, X.B. Sun, Q.M. Ren, L.M. Chen, M.L. Fu, J.L. Wu, D.Q. Ye, Size effect of Pt nanoparticles on the catalytic oxidation of toluene over Pt/CeO_2 catalysts, Appl. Catal. B: Environ. 220 (2018) 462–470.
[59] Q. Zhao, Y.L. Ge, K.X. Fu, Y.F. Zheng, Q.L. Liu, C.F. Song, N. Ji, D.G. Ma, Catalytic performance of the Pd/TiO_2 modified with MnO_x catalyst for acetone total oxidation, Appl. Surf. Sci. 496 (2019) 143579.
[60] S.H. Li, C. Zhang, C.L. Wu, H.F. Zhang, X.H. Yan, Pd/CeO_2/γ-Al_2O_3 catalyst with low loading for catalytic oxidation of VOCs, J. Inorg. Mater. 34 (2019) 827–833.
[61] Z.W. Wang, S. Li, S.H. Xie, Y.X. Liu, H.X. Dai, G.S. Guo, J.G. Deng, Supported ultralow loading Pt catalysts with high H_2O-, CO_2-, and SO_2- resistance for acetone removal, Appl. Catal. A Gen. 579 (2019) 106–115.
[62] N. Burgos, M. Paulis, M.M. Antxustegi, M. Montes, Deep oxidation of VOC mixtures with platinum supported on Al_2O_3/Al monoliths, Appl. Catal. B: Environ. 38 (2002) 251–258.
[63] Z.B. Rui, M.N. Tang, W.K. Jia, J.J. Ding, H.B. Ji, Insight into the enhanced performance of TiO_2 nanotube supported Pt catalyst for toluene oxidation, Catal. Today 297 (2017) 159–166.
[64] H. Sun, Z.G. Liu, S. Chen, X. Quan, The role of lattice oxygen on the activity and selectivity of the OMS-2 catalyst for the total oxidation of toluene, Chem. Eng. J. 270 (2015) 58–65.
[65] H. Einaga, K. Mochiduki, Y. Teraoka, Photocatalytic oxidation processes for toluene oxidation over TiO_2 catalysts, Catalysts 3 (2013) 219–231.
[66] W.C. Xu, N. Wang, Y.D. Chen, J.D. Chen, X.X. Xu, L. Yu, L.M. Chen, J.L. Wu, M.L. Fu, A.M. Zhu, D.Q. Ye, In situ FT-IR study and evaluation of toluene abatement in different plasma catalytic systems over metal oxides loaded γ-Al_2O_3, Catal. Commun. 84 (2016) 61–66.
[67] J. Li, H.B. Na, X.L. Zeng, T.L. Zhu, Z.M. Liu, In situ DRIFTS investigation for the oxidation of toluene by ozone over Mn/HZSM-5, Ag/HZSM-5 and Mn-Ag/HZSM-5 catalysts, Appl. Surf. Sci. 311 (2014) 690–696.
[68] Y.N. Liao, X. Zhang, R.S. Peng, M.Q. Zhao, D.Q. Ye, Catalytic properties of manganese oxide polyhedra with hollow and solid morphologies in toluene removal, Appl. Surf. Sci. 405 (2017) 20–28.
[69] S. Besselmann, E. Loffler, M. Muhler, On the role of monomeric vanadyl species in toluene adsorption and oxidation on V_2O_5/TiO_2 catalysts: a Raman and in situ DRIFTS study, J. Mol. Catal. A Chem. 162 (2000) 401–411.
[70] W.C. Xu, X.X. Xu, J.L. Wu, M.L. Fu, L.M. Chen, N. Wang, H.L. Xiao, X.F. Chen, D.Q. Ye, Removal of toluene in adsorption–discharge plasma systems over a nickel modified SBA-15 catalyst, RSC Adv. 6 (2016) 104104–104111.
[71] L. Li, C.B. Zhang, H. He, J.X. Liu, An integrated system of biological and catalytic oxidation for the removal of o-xylene from exhaust, Catal. Today 126 (2007) 338–344.
[72] M. El-Maazawi, A.N. Finken, A.B. Nair, V.H. Grassian, Adsorption and photocatalytic oxidation of acetone on TiO_2: an in situ transmission FT-IR study, J. Catal. 191 (2000) 138–146.
[73] M.A. Hasan, M.I. Zaki, L. Pasupulety, Oxide-catalyzed conversion of acetic acid into acetone: an FTIR spectroscopic investigation, Appl. Catal. A Gen. 243 (2003) 81–92.
[74] J. Szanyi, J.H. Kwak, Photo-catalytic oxidation of acetone on a TiO_2 powder: an in situ FTIR investigation, J. Mol. Catal. A Chem. 406 (2015) 213–223.
[75] A. Mattsson, M. Leideborg, K. Larsson, G. Westin, L. Osterlund, Adsorption and solar light decomposition of acetone on anatase TiO_2 and niobium doped TiO_2 thin films, J. Phys. Chem. B 110 (2006) 1210–1220.
[76] Z.P. Qu, S.J. Shen, D. Chen, Y. Wang, Highly active Ag/SBA-15 catalyst using post-grafting method for formaldehyde oxidation, J. Mol. Catal. A Chem. 356 (2012) 171–177.
[77] M. Aghbolaghy, J. Soltan, R. Sutarto, The role of surface carboxylates in catalytic ozonation of acetone on alumina-supported manganese oxide, Chem. Eng. Res. Des. 128 (2017) 73–84.
[78] J. Chen, X. Chen, W.J. Xu, Z. Xu, J.Z. Chen, H.P. Jia, J. Chen, Hydrolysis driving redox reaction to synthesize Mn-Fe binary oxides as highly active catalysts for the removal of toluene, Chem. Eng. J. 330 (2017) 281–293.
[79] Z.X. Wu, J.G. Deng, Y.X. Liu, S.H. Xie, X.T. Zhao, Y. Jiang, J. Yang, H. Arandiyan, G.S. Guo, H.X. Dai, Three-dimensionally ordered mesoporous Co_3O_4-supported Au-Pd alloy nanoparticles: high-performance catalysts for methane combustion, J. Catal. 332 (2015) 13–24.